CHARACTERISTICS OF HYPERVELOCITY IMPACT CRATERS ON LDEF EXPERIMENT S1003 AND IMPLICATIONS OF SMALL PARTICLE IMPACTS ON REFLECTIVE SURFACES

Michael J. Mirtich
Sharon K. Rutledge
Bruce A. Banks
NASA Lewis Research Center
Cleveland, Ohio

Christopher De Vries
Cornell University
Ithaca, New York

and

James E. Merrow
Cleveland State University
Cleveland, Ohio

SUMMARY

The Ion Beam Textured and Coated Surfaces Experiment (IBEX), designated S1003, was flown on LDEF at a location 98 degrees in a north facing direction relative to the ram direction. Thirty-six diverse materials were exposed to the micrometeoroid (and some debris) environment for 5.8 years. Optical property measurements indicated no changes for almost all of the materials except S-13G, Kapton, and Kapton-coated surfaces, and these changes can be explained by other environmental effects. From the predicted micrometeoroid flux of NASA SP-8013, no significant changes in optical properties of the surfaces due to micrometeoroids were expected. There were hypervelocity impacts on the various diverse materials flown on IBEX, and the characteristics of these craters were documented using scanning electron microscopy (SEM). The S1003 alumigold-coated aluminum cover tray was sectioned into 2 cm x 2 cm pieces for crater documentation. The flux curve generated from this crater data fits well between the 1969 micrometeoroid model and the Kessler debris model for particles less than 10^{-9} gm which were corrected for the S1003 position (98° to ram). As the particle mass increases, the S1003 impact data is greater than that predicted by even the debris model. This, however, is consistent with data taken on intercostal F07 by the Micrometeoroid/Debris Special Investigating Group (M/D SIG). The mirrored surface micrometeoroid detector flown on IBEX showed no change in solar reflectance and corroborated the S1003 flux curve, as well as results of this surface flown on SERT II and OSO III for as long as 21 years.

INTRODUCTION

The Ion Beam Textured and Coated Surfaces Experiment (IBEX) was designated S1003 on LDEF at a location 98 degrees relative to the ram direction in a north facing direction (ref. 1). Thirty-six diverse materials were exposed to the micrometeoroid and debris (M/D) environment for 5.8 years. Optical property measurements indicated no changes for almost all of the materials except S-13G (zinc oxide in a silicone binder), Kapton-H, and Kapton-H-coated surfaces, and these changes can be explained by other environmental effects. From the predicted micrometeoroid flux of NASA SP-8013, no changes in optical properties of the surfaces due to micrometeoroids were expected. However, there were hypervelocity impacts on the various diverse materials flown on IBEX. The characteristics of these craters were documented using SEM and are presented in the first section of this paper.

The S1003 tray cover was (alumigold coated, [chromic conversion process] Al type 6061 T6), 48 cm x 48 cm. An analysis using the micrometeoroid flux curve of Cour-Palais (ref. 2) and debris model of Kessler (ref. 3), indicated that there was sufficient area to generate a statistically meaningful M/D flux curve for particles of 10^{-6} cm or less. Because of the stabilized orientation of LDEF, a directional M/D flux curve could be obtained at 98° to the ram direction. With this in mind, the tray was sectioned into 690 pieces, 2 cm x 2 cm, for crater documentation. The flux curve thus generated could then be compared to both M/D fluxes of references 2 and 3, as well as other M/D data taken by other LDEF investigators. This is presented in the second part of the paper.

Interest in placing large solar concentrator/solar dynamic systems in space for power generation has brought up a concern for maintaining the integrity of the optical properties of highly specular reflecting surfaces in the near-Earth space environment. It has been shown that highly reflective polished metals and thin film coatings degrade when exposed to simulated micrometeoroids in the laboratory (ref. 4). At NASA Lewis Research Center, a shock tube was used to simulate the phenomenon of micrometeoroid impact by accelerating micron-sized particles to hypervelocities. Any changes in the optical properties of surfaces exposed to this impact were then evaluated. A calibrated sensor (2,000Å of Al/stainless steel) was developed to not only detect the small size micrometeoroid environment, but also to evaluate the degradation of the optical properties of thin aluminum films in space. This sensor (coated by G. Hass of Army Research and Development Center in 1963 of vapor-deposited Al) was flown on LDEF experiment S1003 and also on the OSO III and SERT II satellites that were launched in 1967 and 1970, respectively. The results of these experiments are also presented in this paper, and the relevance of the M/D fluxes on the optical properties of highly reflective surfaces is discussed.

RESULTS AND DISCUSSION

Characteristics of Craters in Various IBEX Surfaces

The largest crater found on the S1003 aluminum tray cover was 1478 micrometers (μm) as measured from outer lip edge to outer lip edge; the inner diameter was 984 μm. Figures 1a and 1b show the crater lip and the crater itself. EDAX of material in the crater indicates that it was caused by a debris particle.

Figures 2 through 4 show the characteristics of craters formed on ion beam textured metals (Cu, Ti, and S.S. type 304). The surfaces were textured to obtain high solar absorptance (α_s) or high thermal emittance (ϵ_{th}). Presented in each figure are the surface texture of the metal and two views of an impact crater. A hypervelocity particle impacting the surface removes the texture in the crater area, but has no effect on the texture beyond the impact crater itself. This is evident in the results of the measurement of the optical properties of the textured surfaces, for there were no measured changes (within the 2% accuracy of the instruments used for the measurements) in the values of α_s or ϵ_{th} of the textured surfaces after 5.8 years of exposure on LDEF.

Figures 5 and 6 show impact craters in black chrome and Grafoil. Again the impact crater affects only the cratered area and does not extend beyond the crater itself. So little of the area of the surface was impacted that the values of α_s and ϵ_{th} again remained unchanged.

Figures 7a-7e contain SEM photomicrographs of M/D impact sites observed on the coated Kapton samples (ref. 1, 5). The largest observed impact was on the 4% PTFE-96% SiO$_2$ sample (figure 7a). This appeared to be an impact by either a collection of particles or one large loosely distributed or extended particle. Another impact site on the same sample (figures 7b and 7c) is of a much smaller diameter. It appears that the type of damage is very dependent on particle size and probably particle velocity. Large impact areas appear to produce delamination, while smaller areas result in a region around the impact which is similar to the splash which is generated by a raindrop in a puddle (figure 7c). There is cracking around the splash region. Similar types of impacts were observed on the silicon dioxide and aluminum oxide coated Kapton samples (figures 7d and 7e). It appears that the impact site morphology is not dependent on the coating composition for these coatings and substrate materials since an area of delamination at an impact site on an aluminum oxide coated Kapton (ref. 5) sample flown on STS-8 looks similar to that on the 4% PTFE-96% SiO$_2$ coated Kapton. It appears that the area of crack damage or delamination is limited in extent for the impact crater sizes observed (ref. 5). In all cases the damage was contained within a diameter less than three times the impact crater diameter. This is very encouraging for the use of protective coatings in LEO since the damage that will result from an impact is small and thus not a significant cause for atomic oxygen attack of the underlying material.

S1003 Cumulative Flux Calculations

To evaluate the micrometeoroid and debris fluxes in lower earth orbit, the cover tray to experiment S1003 flown on the Long Duration Exposure Facility (LDEF) was cut into 690 samples, 2 cm x 2 cm, which were scanned randomly for craters. The total surface area of the cover tray is 0.17396 square meters. One hundred and eighty-five samples (0.044258 square meters) were scanned at 128 times magnification in order to find craters greater than or equal to 20 microns in diameter. Three hundred and twenty-three such craters were found. Two hundred and fifty-six samples (0.062543 square meters) were scanned at 80 times magnification in order to find craters greater than or equal to 38 microns in diameter. One hundred and thirty such craters were found. Then the remaining samples were scanned at 44 times magnification in order to find craters greater than or equal to 58 microns in diameter. One hundred and forty-eight craters greater than or equal to 58 microns in diameter have been found.

In order to plot the crater data as a cumulative flux curve as a function of particle mass, the following assumptions were made: the ratio of crater diameter to particle diameter is 5 to 1, which is the criteria used by the M/D SIG (ref. 6), and the particle density in low Earth orbit varies with respect to particle mass based on Kessler's meteoroid (ref. 6) and debris (ref. 3) models. These models assume that the particle density varies from a high of 2.5 gm/cc at 10^{-10} gm to 1.4 gm at 10^{-6} gm. Figure 8 shows a plot of the S1003 data for LDEF row 6 along with the standard deviation error range that is based on the S1003 cover tray area.

The results of the S1003 cover tray cumulative flux measurements can be compared to recent debris and meteoroid models corrected for LDEF row 6 as well as data from other parts of the LDEF.

The cumulative flux of debris in lower earth orbit is believed to follow the following equation (ref. 3):

$$F(d,h,i,t,S) = k \cdot \phi(h,S) \cdot \psi(i) \cdot [F_1(d) \cdot g_1(t) + F_2(d) \cdot g_2(t)] \tag{1}$$

where

F = flux in impacts per square meter of surface per year
k = 1 for a randomly tumbling surface; must be calculated for a directional surface
d = orbital debris diameter in cm
t = time expressed in years
h = altitude in km (h < 2000 km)
S = 13-month smoothed 10.7 cm-wavelength solar flux expressed in 10^4 Jy (1 Jy = 10^{-26} Watts per square meter per hertz); retarded by 1 year from t
i = inclination in degrees

and

434

$$\phi(h,S) = \frac{\phi_1(h,S)}{\phi_1(h,S) + 1}$$

$$\phi_1(h,S) = 10^{\frac{h}{200} - \frac{S}{140} - 1.5}$$

$$F_1(d) = 1.05 \times 10^{-5} \cdot d^{-2.5}$$

$$F_2(d) = 7.0 \times 10^{10} \cdot (d+700)^{-6}$$

$$g_1(t) = (1 + 2 \cdot p)^{(t-1985)}$$

$$g_2(t) = (1 + p)^{(t-1985)}$$

p = the assumed annual growth rate of mass in orbit

The values for $\Psi(i)$, the flux enhancement factor, are given in Table 1 of reference 1 and depend on the inclination angle (i) of a surface.

The following assumptions were made for the LDEF:

h = 450 km (Rough average)

S = 115 (Rough average)

p = 10%

k = 1.24 (for LDEF row 6 on which experiment S1003 was flown. Row 6 was consistently 98° from ram direction.)

i = 28.5°

t = 1987 (Midpoint of LDEF mission)

    With these assumptions, the debris model for row 6 is plotted in figure 8.
    There are two meteoroid environment models which can be used to estimate the cumulative flux of meteoroids in low earth orbit. The first of these will be referred to as the 1969 model (ref. 2). The second will be referred to as the 1970 model (ref. 7). The 1969 model is designed to predict the meteoroid flux near the earth and moon, while the 1970 model is designed to cover the entire solar system. The 1969 model presents the following equation to determine cumulative flux.

$$\log_{10}N_t=-14.37-1.213\log_{10}m \qquad (2)$$

for

$$10^{-6}\leq m\leq 10^{0}$$

and

$$\log_{10}N_t=-14.399-1.584\log_{10}m-0.063(\log_{10}m)^2 \qquad (3)$$

for

$$10^{-12}\leq m\leq 10^{-6}$$

where

N_t = number of particles of mass m or greater per square meter per second

m = particle mass in grams

The cumulative 1969 micrometeoroid flux (N_t) was adjusted for the Earth's gravitational effect and the shielding of meteoroids by the Earth (ref. 2). The 1970 model presents a more complex way of finding cumulative flux curves in low Earth orbit as well as a different equation for calculating the effect of a planet's gravitation on the flux of meteoroids. The results of the calculations of both the 1969 model and the 1970 model for low Earth orbit are presented in figure 9. The 1969 and 1970 models are each presented before taking the effects of gravity and planetary shielding into account (the uncorrected curves), and the models are presented after taking the effects of gravity and planetary shielding into account (the corrected curves). The corrected 1969 model was chosen because it is easier to perform the required calculations to find the flux curve, and because it produces a curve practically indistinguishable from the corrected 1970 model.

Figure 8, therefore, shows a comparison of the S1003 data to the corrected debris and meteoroid models, for LDEF row 6. At low particle mass (10^{-9} gm), the S1003 impact data fits between the debris and micrometeoroid models. As the particle mass increases, the S1003 impact data is greater than that predicted by even the debris model.

However, comparisons between the S1003 cover tray and other parts of the LDEF indicate that there may have been a localized area where the particle flux was greater than usual. Figure 10 shows a comparison of the S1003 cover tray to Intercostals B06 and F07. S1003 does show a flux similar to that for intercostal F07 which was located on row 7, but closer to experiment S1003 than intercostal B06. Of course, the S1003 crater impact data is preliminary, and has not as yet been separated for debris or

436

micrometeoroid particles. This will be determined by the use of secondary ion mass spectrometry (SIMS), after which flux curves for debris and micrometeoroids for row 6 will be generated.

Implication of Micrometeoroid and Space Debris Models and Erosion of Surface Optical Properties

The micrometeoroid detector flown on IBEX was a 2000Å layer of Al vapor deposited on stainless steel. This surface has a long history in space and was ground calibrated in the 1960's when the majority of the micrometeoroid sensors (capacitor discharge or microplane sensors) had little or no such calibration (ref. 8).

A shock tube was used to accelerate $(2-14)\mu$ SiC particles to high enough speeds such that hypervelocity impact occurred in metals.[4] A series of polished metal discs composed of Al, stainless steel, and 1900Å Al on stainless steel substrates were chosen as potential materials for a space flight experiment. The discs, 4.45 cm^2, were progressively exposed to increasing amounts of simulated micrometeoroid exposure. Spectral reflectance measurements on all the discs were made before and after exposure to the simulated micrometeoroids. A typical reduction in spectral reflectance between 1.5 and 15.5 microns is shown in figure 11, for 1900Å Al on stainless steel after exposure to 0.22 J/cm^2 of 6 μ SiC particles travelling at 2.65 km/sec where the energy density is given as:

$$Energy\ Density = \sum \frac{\tfrac{1}{2}\,m_i v_i^2}{area} \qquad (4)$$

To obtain average reflectance values (for the sake of comparison), spectral reflectance data were weighted for the energy distribution corresponding to a 420 K blackbody. In figure 12, all of the average reflectance ratios for stainless steel, aluminum, and aluminum on stainless steel are plotted against the total energy of the impacting particles.

The data in figure 12 indicate that the reduction in the infrared reflectance ratio of aluminum is somewhat greater at any exposure than that of stainless steel. The reflectance of both, however, falls to less than 60% of the original value after only 7.5 J (1.65 J/cm^2) of laboratory exposure.

A space-environment-simulation facility was used to determine the equilibrium temperature of the surfaces presented in figure 12. In the working section of the inner "space" chamber, which was six feet in diameter and approximately ten feet high, four characteristics of the space environment were reproduced simultaneously and as accurately as possible. The four were: the low pressure of gases in space, estimated to be about 10^{-14} mm Hg., low background temperature (4°K), very nearly perfect absorption capability of space background for gases (blackened walls at LHe temperature), and sun radiation at proper intensity, uniformity, and collimation angle, as well as spectral distribution from .35 to 2.5 mm.

The "history" of the equilibrium temperature for discs composed of three different materials mounted on a simulated space vehicle and "flown" in the simulated space environment at 1.25 solar constant can be found in figure 13. These equilibrium temperatures are shown as they vary with exposure to the simulated micrometeoroid environment. The exposure is expressed in joules per square centimeter of energy of the impacting hypervelocity particles on the 2.38 cm diameter discs. The resulting variation in the equilibrium temperatures for all the discs is the result of reproducible changes in surface optical properties (α_s and ϵ_{th}) caused by calibrated exposure to high-speed, micron-sized particle impact. Perhaps the most important feature of these curves is that in spite of the large exposure to impacting particles, the resulting change in optical properties measured in the laboratory, and the efforts made to isolate the disc thermally from its support, the total variation in equilibrium temperature of the discs is small but measurable. For the aluminum disc, the measured change in equilibrium temperature is approximately 21 K or about 5% in absolute temperature level. For stainless steel, the temperature is almost constant, varying only about 0.1% in absolute temperature level. The largest variation occurred with the aluminum-coated stainless steel disc, which rose 50 K due to the exposure, or about 12% in absolute temperature level.

It was found in reference 8 that there was a similarity in the variation of reflectance with simulated micrometeoroid exposure as measured either by direct measurement of α_s or ϵ_{th} using optical spectrophotometers or by use of the equilibrium temperature method of a space simulation chamber (ref. 8). This suggested the possibility of making reflectance measurements in space without a reflectometer and using these reflectance measurements to determine the micrometeoroid flux.

This could be done by calibrating the change in temperature of a disc in a space-environment-simulation chamber with the measured (elsewhere) optical change of the surface caused by calibrated exposure of the disc to simulated micrometeoroid flux. Consequently, telemetering the temperature of the disc from a space experiment would give not only the change in reflectivity of the disc, but also, from correlation with the ground experiment, the micrometeoroid flux causing this reflectivity change. The surface chosen for space-flight experiments, because of its initial fast rise in equilibrium temperature and large changes initially in α_{sn} and ϵ_{th} when exposed to simulated micrometeoroids, (see fig. 13) was the 1900Å Al/stainless steel disc. Discs with 2000Å of Al/SS were placed thermally isolated from the spacecraft on OSO III and SERT II. Reference 9 describes the Reflection Erosion Experiment (REX) on the SERT II spacecraft in detail. The results of 21 years of exposure of the REX on SERT II, which was in a 1000 km polar orbit, will be highlighted here.

Figure 14 is a time plot of REX disc #2 temperature from launch of SERT II (February 1970) to July 1990. The shaded areas of figure 14 represent times when the spacecraft was intermittently shadowed by the earth. The disc temperatures in

438

figure 14, which were normalized to constant REX body temperature of 316 K and zero angle of sun incidence, show almost no long-term change or trend after 21 years in space.

Figure 15 is a plot of REX disc α_{sn} values calculated using actual values of REX disc and body temperatures, solar flux as a function of angle of incidence, day of the year, a heat transfer K of 14.8 x 10^{-12} J/sec-K^4 between disc and body, and a disc thermal emittance of 0.017 (ϵ_{th}) (ref. 8). The above-described parameters were combined in equation (B3) of reference 8 for each individual point taken, and a value of α_{sn} was calculated. The disc surface material (2000Å Al/SS) and temperature level were chosen to make the REX α_{sn} sensitive and not ϵ_{th} sensitive.

The initial launch value of α_{sn} was 0.111, as measured in ground testing. The initial value of α_{sn} measured in space was the same. The value of α_{sn} increased in the first two months in space to 0.128, and then levelled off at 0.134. As the sun angle of incidence increased in late 1970 and during 1971, the calculated α_{sn} value was reduced to about 0.120. The value of α_{sn} remained at 0.120 from 1979 to 1981. The scatter of α_{sn} values was probably caused by the spinning spacecraft and a ±5° uncertainty of the sun angle of incidence. At the next opportunity to obtain data, July, 1989, α_{sn} had increased to a value of about 0.130.

The changes in α_{sn} were quite small (0.11 to 0.13) over a 21-year period in space, compared to the change of 0.11 to 0.40 in 12 months predicted by the 1963 High Micrometeoroid Flux Model[10] was correct. The major result was that there has been no major change in disc temperature or α_{sn} over a 21-year period in space. This result indicates that the Micrometeoroid Flux Model of 1963 was considerably higher than the actual flux. The results are in better agreement with the 1969 Micrometeoroid Flux Model[10] and the 1987 Orbital Debris Model of Laurance and Brownlee.[11]

From the accuracy of the sensor, these results indicate that a reflector surface (a highly polished metal or thin metal film deposit) should lose less than 1% of its specular reflectance in near-Earth orbit over 21 years. This is an important factor in the design of space solar dynamic/concentrator systems. An extrapolation based on area damage derived from the 1969 Micrometeoroid Model and ground reduction in specular reflectance due to micrometeoroid simulation studies indicate that such a reduction of specular reflectance should not happen within the useful lifetime of currently conceived space systems.

CONCLUDING REMARKS

Thirty-six diverse materials were flown on S1003 at 98° (northward) relative to the ram direction. There were no changes in optical properties of the surfaces due to the micrometeoroid or debris environment. Characteristics of the hypervelocity craters formed in ion beam textured metals show that the hypervelocity particles impacting the surface removed the texture in the crater, but had no effect on the texture beyond the impact crater itself. This indicates that a surface textured to obtain select optical properties will retain those properties because the surface area impacted by micrometeoroids or debris particles is so small (area damaged = 10^{-4} x original area after 21 years in space).

A comparison of the S1003 cover tray hypervelocity flux data to the 1969 micrometeoroid and debris models corrected for LDEF row 6, show that for low particle mass (10^{-9} gm) the S1003 impact data fits between the debris and the micrometeoroid models. However, as the particle mass increases, the S1003 impact data is greater than that predicted by even the debris model. Comparisons between the S1003 cover tray and an intercostal on row 6 indicate that there may have been a localized area where the particle flux was greater than usual.

The mirrored surface (micrometeoroid detector) showed no change in solar reflectance and corroborated the results of this surface flown on OSO III and SERT II for as long as 21 years. This data does indicate that a reflector surface should lose less than 1% of its specular reflectance after 21 years in near-Earth orbit.

REFERENCES

1. Mirtich, M. J., Rutledge, S. K., Stevens, N., Olle, R., and Merrow, J., "Ion Beam Textured and Coated Surfaces Experiment (IBEX)," Proceedings of 1st LDEF Post-Retrieval Symposium, Kissimmee, FL, June 2-8, 1991, pp. 989-1004.

2. Cour-Palais, B. G., "Meteoroid Environment Model - 1969 [Near Earth to Lunar Surface]," NASA SP-8013, 1969.

3. Kessler, D. J., Reynolds, R. C., Anz-Meador, P. D., "Orbital Debris Environment for Spacecraft Designed to Operate in Low Earth Orbit," NASA TM 100471, 1989.

4. Mirtich, M. J., and Mark, H., "Feasibility of Accelerating Microns Size Particles in Shock Tube Flows for Hypervelocity Degradation of Reflective Surfaces," NASA TND-3187, January 1966.

5. Rutledge, S. K., and Olle, R. M., "Durability Evaluation of Photovoltaic Blanket Materials Exposed on LDEF Tray S1003," Proceedings of 1st LDEF Post-Retrieval Symposium, Kissimmee, FL, June 2-8, 1991.

6. Personal Communication by M/D SIG Members, M. Mirtich and M. Zolensky, at M/D SIG Meeting, Houston, TX, March 1992.

7. Kessler, D. J., "Meteoroid Environment Model - 1970 [Interplanetary and Planetary]," NASA SP-8038, 1970.

8. Mark, H., Summers, R. D., and Mirtich, M. J., "Effect on Surface Thermal Properties of Calibrated Exposure to Micrometeoroid Environment," AIAA Journal, 4 (10) (1966), 1811-1818.

9. Mirtich, M. J., and Kerslake, W. R., "The Effect of the Near-Earth Space Environment on a Mirror Surface After 20 Years in Space," TMS Meeting, Los Angeles, CA, February 19-21, 1990, in "Materials Degradation in LEO," edited by Srinivasan and Banks, MMM Society, 1990, pp. 107-122.

10. Alexander, W. M., McCraken, C. W., Secretan, L., and Berg, O. E., "Review of Direct Measurements of Interplanetary Dust from Satellites and Probes," Proceedings of the Third International Space Sciences Symposium, edited by W. Priester (John Wiley and Sons, Inc., N.Y. 1963, Sec C2, Paper 1, 891-917).

11. Cour-Palais, B. G., "Meteoroid Environment Model, Near-Earth to Lunar Surface," NASA SP 8013, 1969.

12. Laurance, M. R., and Brownlee, D. E., "The Flux of Meteoroids and Orbital Space Debris Striking Satellites in Low Earth Orbit," Nature, Vol. 323, 1986, pp. 136-138.

Micrometeoroid Impact
LDEF E06-S1003 Piece #278
Inner Diameter: 984 micrometers
Crater Edge to Edge: 1476 micrometers
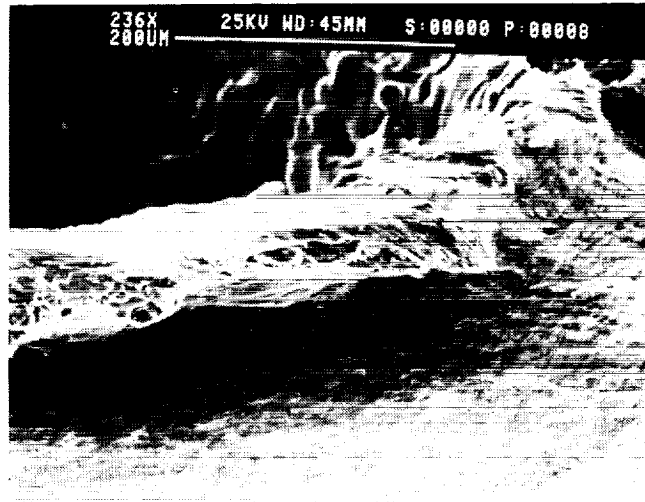
(a)
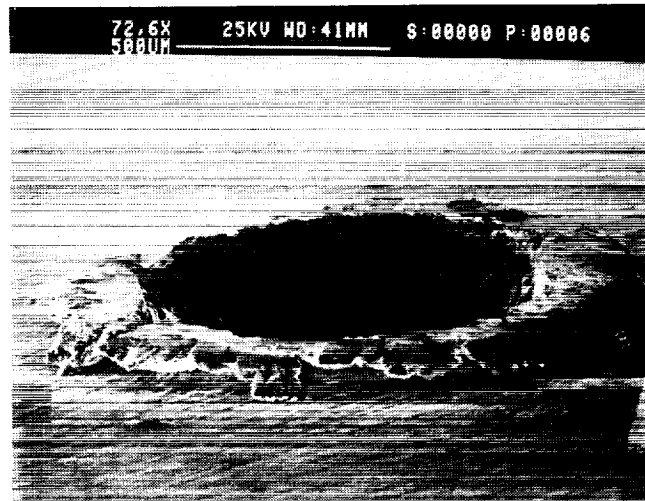
(b)

1. (a and b) Photomicrograph of largest crater found on S1003.
    Depicts the lip and crater itself.
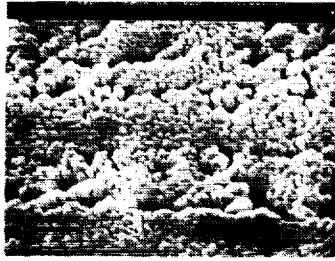
Textured Cu Surface

Impact Crater

Impact Crater

2.   Photomicrograph showing textured copper and two different views of an impact crater.
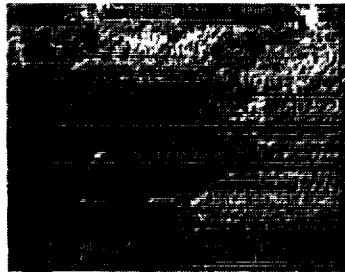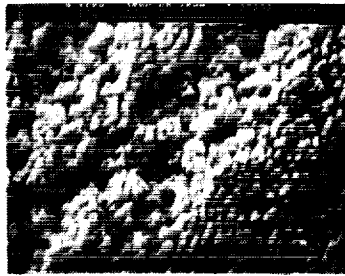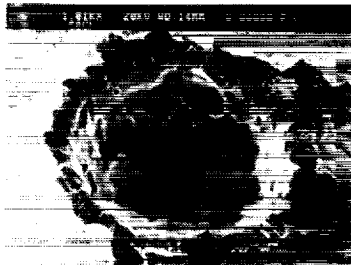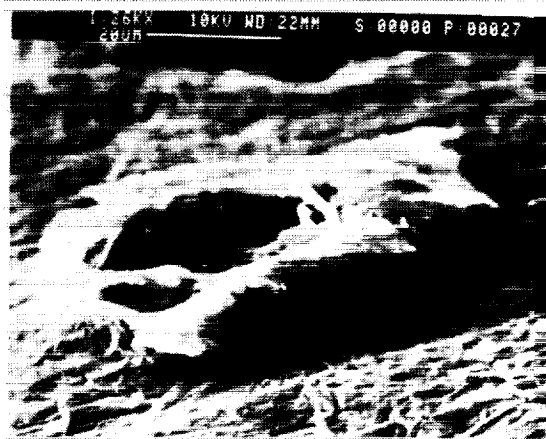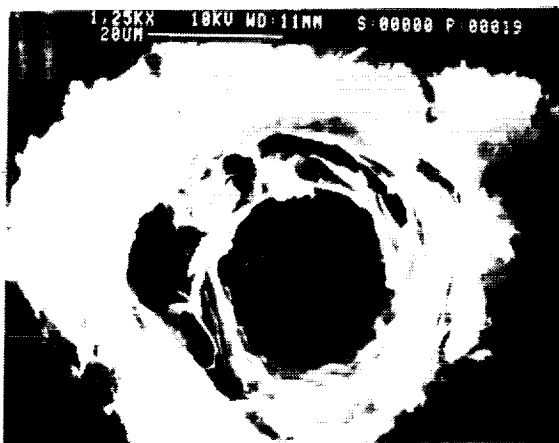

Textured Ti Surface
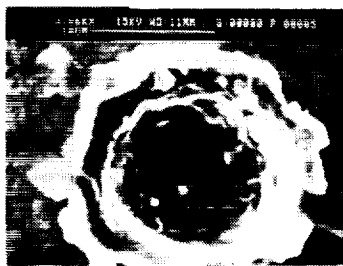
Impact Crater

Impact Crater

3.   Photomicrograph showing textured titanium and two views of an impact crater.

Textured Stainless Steel Surface

Impact Crater

Impact Crater

4. Photomicrograph showing textured stainless steel type 304 and two views of an impact crater.

5. Photomicrograph of impact crater in black chrome.

6.   Impact craters in grafoil.
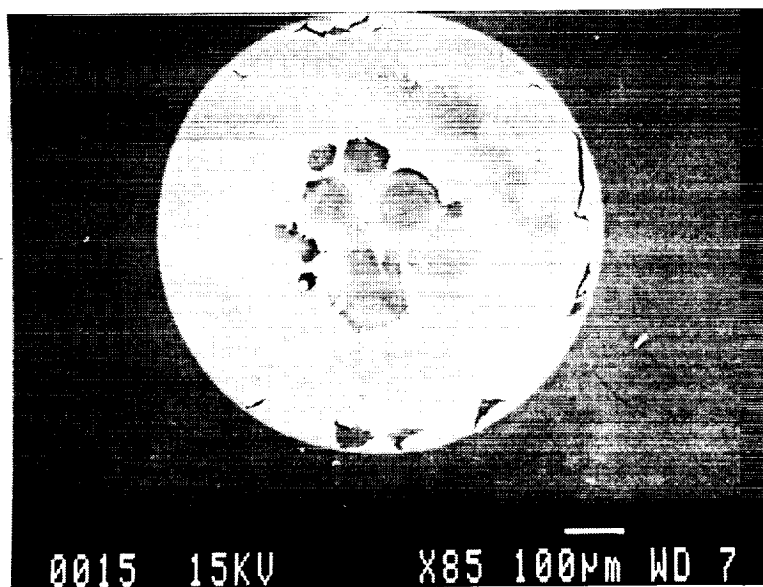
7.   Scanning electron photomicrographs:
      (a)   Conglomerate micrometeoroid or debris impact on 4%
            PTFE-96% SiO_2 coated Kapton.

445
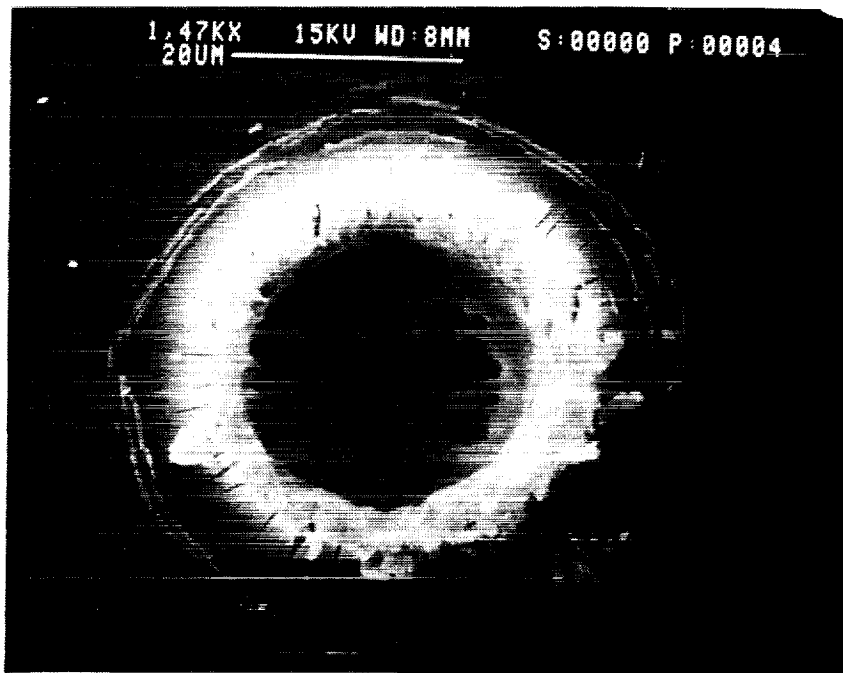
7(b) Micrometeoroid or debris impact on 4% PTFE-96% SiO$_2$ coated Kapton.
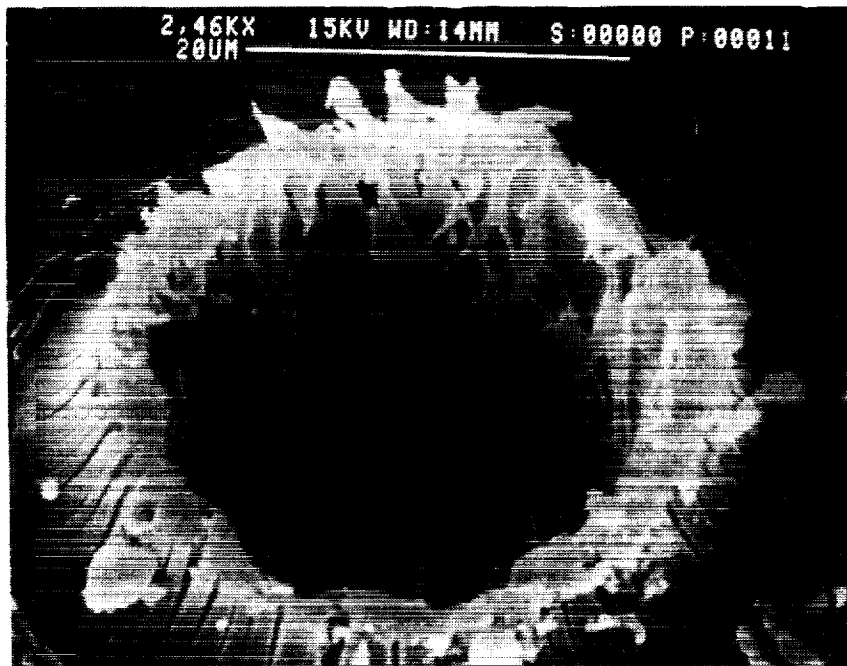
7(c) Micrometeoroid or debris impact on 4% PTFE-96% SiO$_2$ coated Kapton.
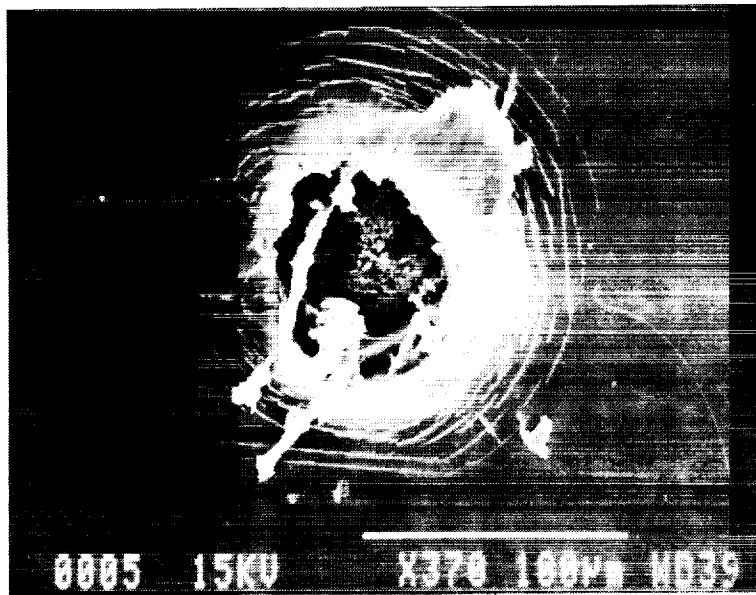
7(d) Micrometeoroid or debris impact on silicon dioxide
       coated Kapton.
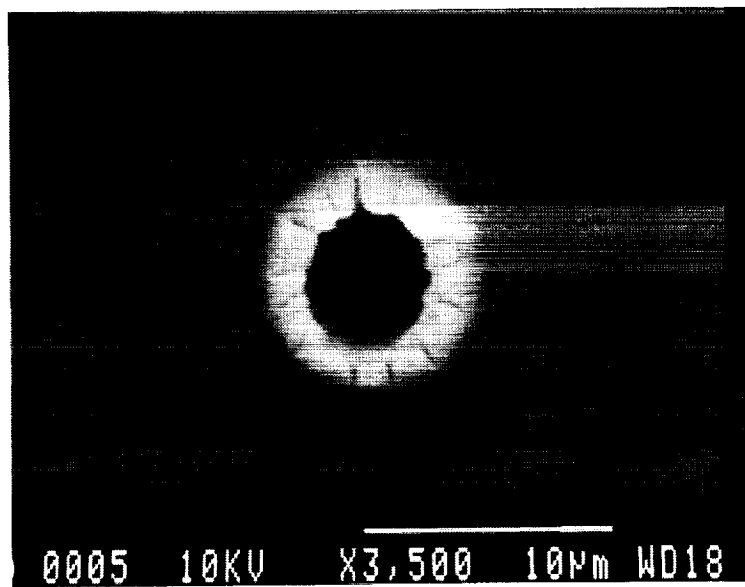
7(e) Micrometeoroid or debris impact on aluminum oxide
       coated Kapton.

447
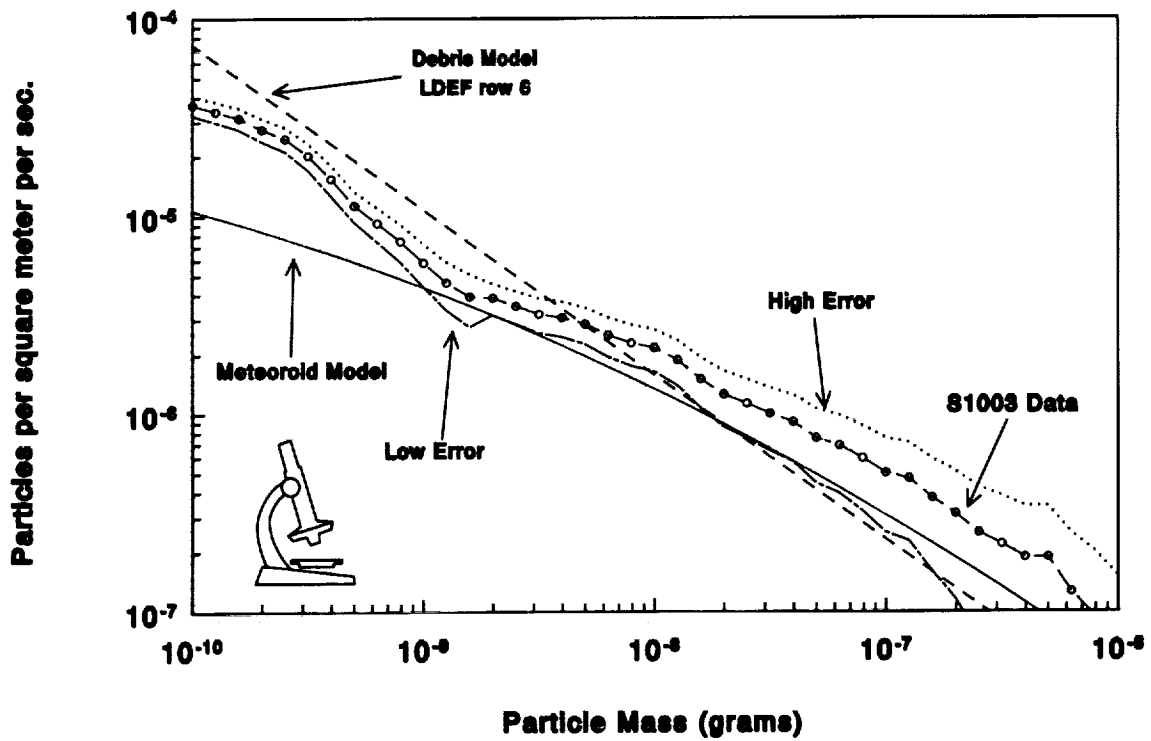
8.   Comparison of S1003 crater data to the corrected debris and
   micrometeoroid models for LDEF row 6.
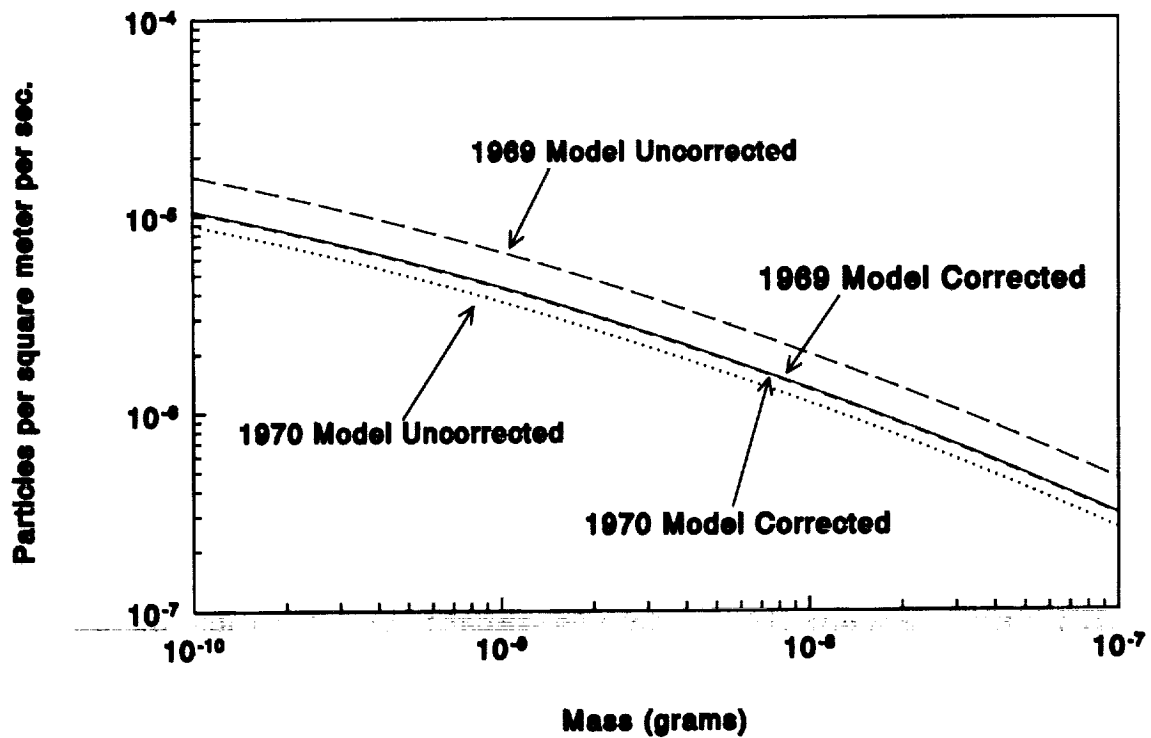
9.   Comparison of 1969 and 1970 micrometeoroid models before and
   after correction for gravity and planetary shielding.
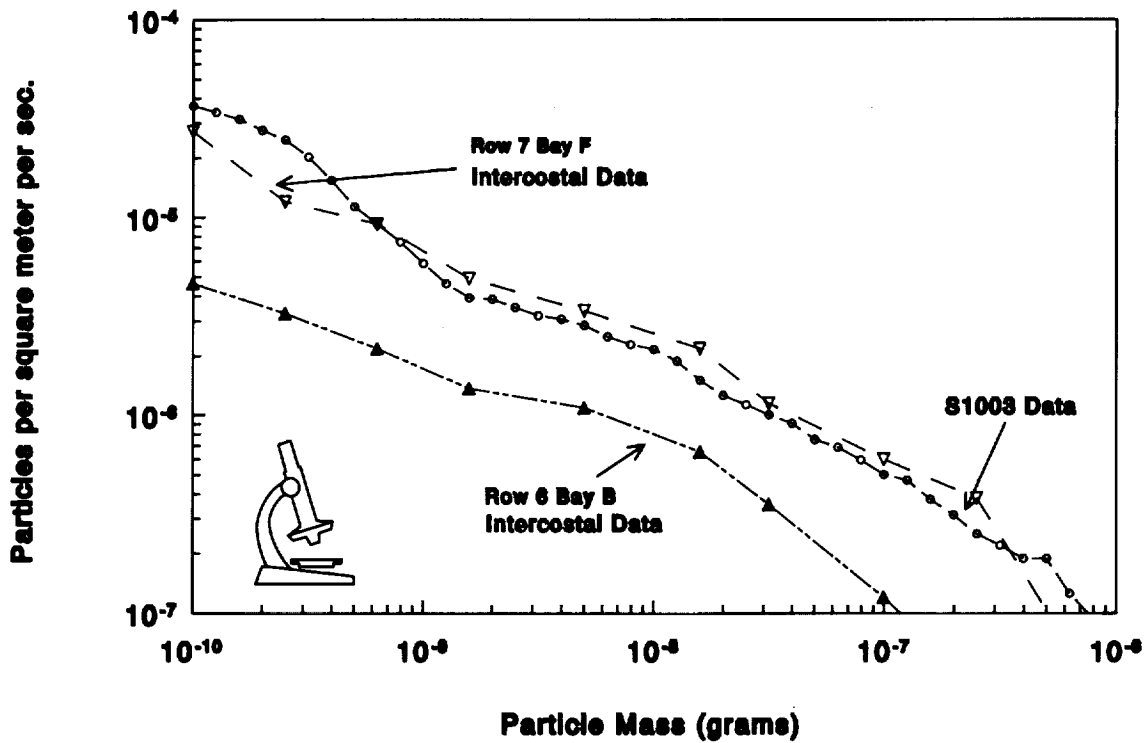
10. Comparison of S1003 data with intracoastal f07 (row 7) and intracoastal (row 6).
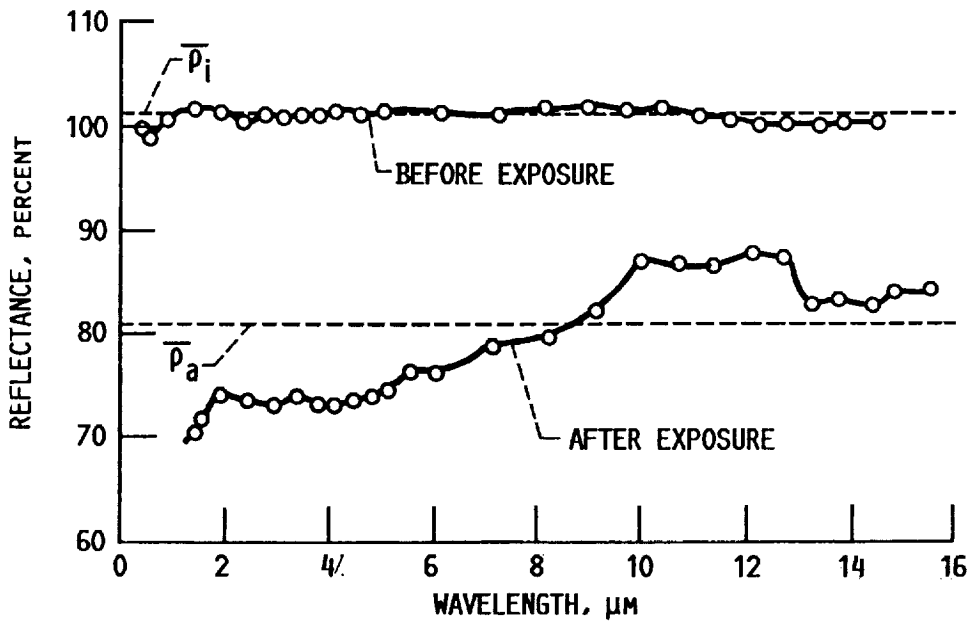

11. Spectral reflectance p_{H-A} for 1900Å aluminum on stainless steel substrate exposed to approximately 0.2 J/cm^2 of hypervelocity impaction.
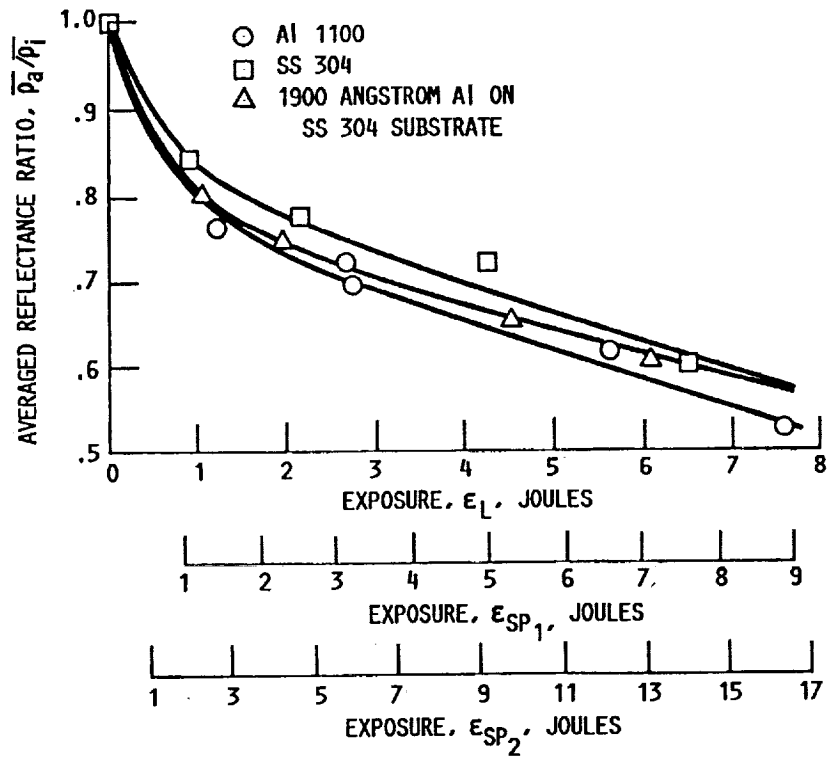
12. Degradation of average reflectance of various metal surfaces after exposure to impaction by 6-μm SiC particles traveling at 8500 ft/s in the laboratory. (Extra abscissas added to indicate exposure necessary for equal damage in space.)
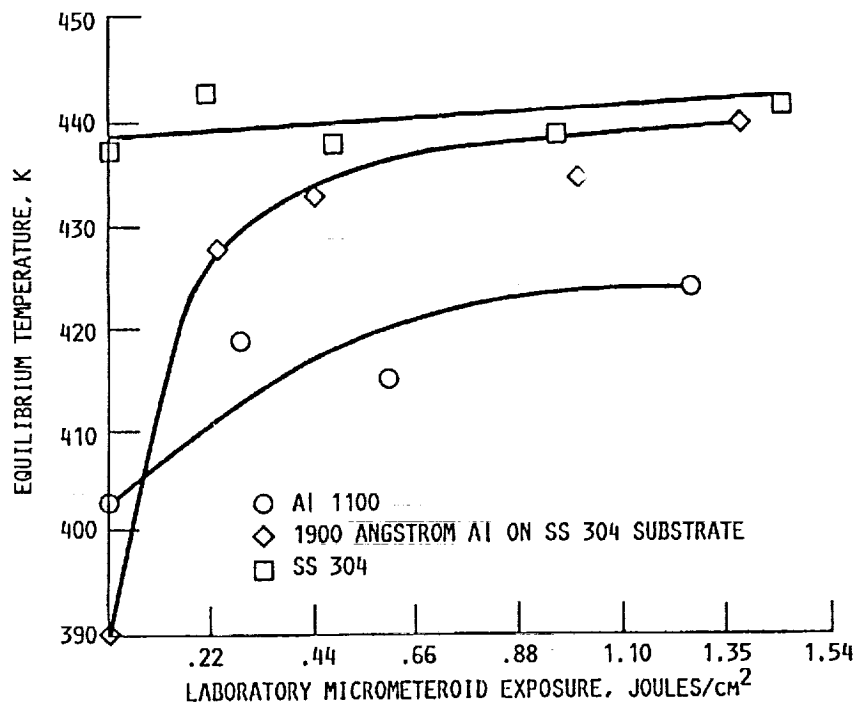
13. Equilibrium temperature as a function of exposure to simulated micrometeoroids.

C-3
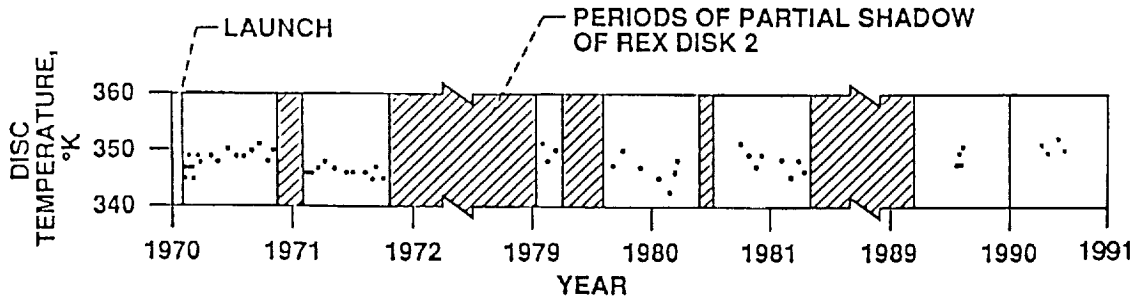
14. REX disk 2 temperature, normalized to constant body temperature (316°K) and zero-incident-sun angle.
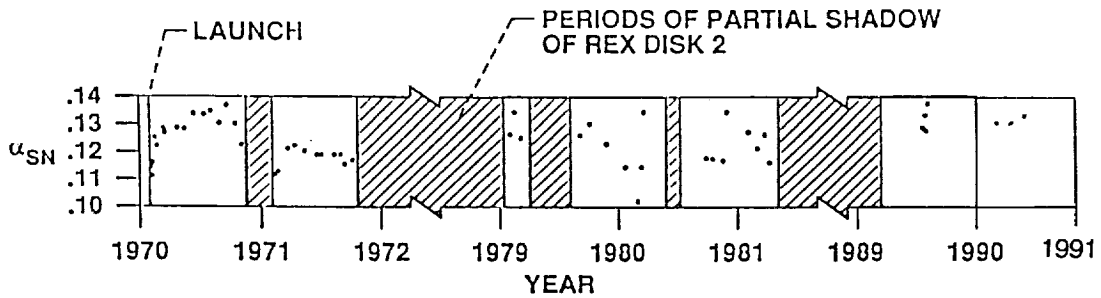
15. Change of solar absorptance (α_{sn}) with time for Al/S.S. (SERT II) disk.